


RESEARCH ARTICLE OPEN ACCESS

Label-Free Detection of π -Stacking Interactions During Tryptophan Self-Assembling Into Amyloid-Like Structures Using Surface-Enhanced Raman Scattering

Gabriel Conishi Cardozo¹ | Evandro Luiz Duarte¹ | Antonio Rodrigues da Cunha^{1,2} | Diogo Soga¹ | Márcia de Almeida Rizzutto¹ | M. Teresa Lamy¹ | Erix Alexander Milán-Garcés¹ 

¹Instituto de Física, Universidade de São Paulo, São Paulo, SP, Brazil | ²Universidade Federal do Maranhão, São Luís, Maranhão, Brazil

Correspondence: Erix Alexander Milán-Garcés (garces@usp.br)

Received: 1 April 2025 | **Revised:** 16 April 2025 | **Accepted:** 29 April 2025

Funding: This work was supported by the São Paulo Research Foundation (FAPESP) (Grant 2021/01593-1) and the National Council for Scientific and Technological Development (CNPq).

Keywords: amyloid fibrils | Raman | self-assembling | SERS | tryptophan

ABSTRACT

The formation of amyloid fibrils by different proteins and peptides is a well-studied topic. In the last decade, it has been reported that metabolites can also self-assemble into amyloid-like fibrils. The aggregation of single amino acids such as phenylalanine, tyrosine, and tryptophan has also been linked to tyrosinemia type II, hypertryptophanemia, and Hartnup diseases. It is a challenge to monitor the intermolecular interactions involved in the supramolecular self-assembling of metabolites in a time-dependent manner. Here, the surface-enhanced Raman scattering (SERS) technique was used to directly probe the changes in the molecular interactions during the self-assembling of tryptophan into amyloid-like structures, particularly in the initial stages. We showed that this simple and label-free nanoplasmonic-based methodology can be used to examine at the molecular level the formation of amyloid-like aggregates as a function of time. Specifically, the technique was shown to be sensitive and provide insights into the formation of hydrogen bonding, π -stacking interactions, and hydrophobicity changes during the self-assembling of tryptophan. Thus, this work can open new possibilities for the applications of SERS to describe in more detail the mechanisms of formation of other metabolites assembled structures, which may be valuable for understanding several related diseases.

1 | Introduction

During the past decades, the topic of protein aggregation into amyloid fibrils has been extensively studied mostly due to its connection to multiple disorders such as Alzheimer's, Parkinson's, and prion diseases [1, 2]. The amyloid fibril structures present generic properties that are independent of the specific amino acid sequences, such as a fibril morphology, abundance of β -sheet secondary structure, and similar electron diffraction pattern [1, 2]. The fibrils also selectively bind to extrinsic fluorescence dyes like Congo red and thioflavin T (ThT). One of the most common ways to monitor the formation of protein amyloid

fibrils is through ThT staining fluorescence assays. Upon excitation at approximately 450 nm, the ThT fluorescence signal increases when bound to an amyloid structure [3, 4]. A more recent, label-free approach for the detection of this type of assembly is through intrinsic fibril fluorescence [5]. The intrinsic fluorescence of amyloid fibrils occurs upon excitation at wavelengths from 360 to 410 nm and is absent in nonfibrillar samples [5]. It has been shown that this property can be used to monitor the formation of amyloid protein aggregates [5], but the exact mechanism responsible for this fluorescence is still under debate [6, 7]. A prominent hypothesis is that the intrinsic emission is related to the hydrogen bonds in the β -sheets structures [7].

This is an open access article under the terms of the [Creative Commons Attribution](https://creativecommons.org/licenses/by/4.0/) License, which permits use, distribution and reproduction in any medium, provided the original work is properly cited.

© 2025 The Author(s). *Journal of Raman Spectroscopy* published by John Wiley & Sons Ltd.

In the last decade, experimental and computational evidences indicate that single metabolites such as aromatic amino acids and nucleic acid bases can also aggregate and form amyloid-like fibril structures with properties similar to those observed for proteins and peptides [8–14]. In 2012, Adler-Abramovich et al. showed that phenylalanine (Phe), at pathological concentrations, can self-assemble into well-ordered amyloid fibrils [8]. Later, Perween et al. and Shaham-Niv et al. observed that tyrosine (Tyr) also self-assembles into ordered fibrillar structures [11, 14]. More recently, Shaham-Niv et al. also observed that tryptophan (Trp) forms fibrillar aggregates with high cytotoxic activity [10]. Interestingly, the amyloid-like structures formed by metabolites also showed intrinsic fluorescence similar to those of protein and peptides, even in the absence of amide or aromatic groups [6, 10, 15, 16]. There is ample evidence that the extrinsic fluorescence can also be used to probe the presence of metabolite amyloid-like fibrils [8, 10, 11, 16, 17].

A lot of efforts have been spent to determine the role of the molecular interactions involved in the self-assembly of metabolites [6, 10, 12, 16–23]. In the case of aromatic amino acids, it has been suggested that the primary interactions responsible for the amyloid-like fibril formation are hydrogen bonding between neighboring molecules and that π - π , CH- π , and hydrophobic interactions influence the structural morphology [17]. From the crystal structure and molecular dynamics (MD) simulations, it has been previously observed that zwitterionic Trp can form a ladder-like structure with a hydrophilic interior and hydrophobic exterior stabilized by π - π and CH- π interactions [10, 12, 19, 24]. In the hydrophilic region, the Trp molecules are bound by hydrogen bonding interactions between carboxylate and amine groups. The crystal structure also shows that there is a hydrophobic region between two layers. The MD simulations study carried out by Uyaver et al. showed that Trp can also self-assemble into pore-like tetrameric structures, which interact through the indole rings [23]. Similar assemblies have also been suggested for Phe by Do et al. and German et al. using ion-mobility mass spectrometry and MD simulations, respectively [18, 22]. In these cases, the tetramers are held together by hydrogen bonding interactions between COO⁻ and NH₃⁺ groups. The pore-like structures may form higher ordered multiple core aggregates throughout hydrophobic, π - π , and CH- π interactions [18]. The mass spectrometry data obtained by Do et al. also suggests the presence of multiple core structures of Phe where π -stacking and hydrophobic interactions may be involved [18].

Apart from MD simulations, the information about the interactions involved in the metabolites self-assemblies has been acquired mainly from crystal structures, infrared spectroscopy, and mass spectrometry [8, 18, 20, 22, 23, 25, 26]. The presence of π - π stacking interactions has also been suggested from NMR spectroscopy [12]. These experimental techniques have been applied principally to the self-assembled structures and not to monitor the aggregation process from the monomeric stage. The kinetic studies of metabolites self-assembling with sufficient temporal resolution are based, till now, in the extrinsic and intrinsic fluorescence [5, 10, 11, 15–17]. However, these fluorescence methods do not provide direct information about several intermolecular interactions, which are crucial to understand

the mechanisms of the formation of amyloid-like structures. Therefore, there is a need for methodologies that can follow the self-assembling kinetics of metabolites from the early stages with the required temporal resolution and structural details at the molecular level. In the specific case of aromatic amino acids, it is important to have probes that can monitor the formation of π - π and CH- π interactions. Although it is known that these interactions play important roles in the structure, stability and function of proteins as well as in the self-assembling of aromatic amino acids, it is challenging to detect them experimentally [17, 27–30].

One technique that has been shown to be sensitive to several intermolecular interactions and solvent accessibility is Raman spectroscopy. Besides that, the technique has been extensively applied to study the folding, unfolding, and aggregation kinetics of proteins and peptides [31–43]. This vibrational spectroscopy method can provide details about changes in the secondary structures and tertiary contacts of proteins and peptides. Normal Raman and its variant, ultra-violet resonance-enhanced Raman spectroscopy (UVRR), have been widely applied to study the structure and kinetics of amyloid fibrils [31–43]. In recent years, the nanoplasmonic counterparts, surface-enhanced Raman scattering (SERS) and tip-enhanced Raman scattering (TERS) have also been increasingly used in the study and detection of amyloid structures [42, 44–49]. In SERS and TERS, the Raman intensity from molecules adsorbed on the surface of the plasmonic nanostructure can be enhanced several orders of magnitude, which in particular conditions allow single-molecule detection [50, 51]. This enhancement arises for the most part from the excitation of a localized surface plasmon that amplifies the electromagnetic field of both incident and scattered light [52]. Despite the widespread use of Raman spectroscopy in protein studies, it has not been previously applied to monitor the kinetics of metabolites self-assembling.

The aim of this work is to demonstrate that Raman spectroscopy and particularly SERS are suitable label-free methodologies to monitor the self-assembling kinetics of metabolites. For that, we have for the first time applied SERS to monitor the kinetics of Trp self-assembling. Trp is a molecular probe systematically used in Raman and other optical spectroscopy techniques [32, 35, 40, 53–66]. Several Raman bands of Trp have been recognized as markers of different intermolecular interactions, structural conformations, and solvent accessibility in proteins [34, 65–69]. Notably, the Raman spectrum of Trp is sensitive to cation- π , π - π , and CH- π interactions, which are difficult to detect experimentally with other techniques [40, 55, 57, 60, 63, 70]. For example, Milán-Garcés et al. monitored the refolding of the protein barstar using UVRR, and the observed changes in Trp Raman markers provided insights about the formation of the protein core, solvent accessibility, and hydrophobicity of the local environment around Trp53 residue [32]. Thus, it is expected that changes in the Raman spectrum would give important insights about crucial interactions involved in the Trp self-assembling process. Here, we showed that several well-known markers in normal Raman and UVRR can also be used in SERS to qualitatively obtain information about the intermolecular interactions involved in the self-assembling of Trp in water. This simple

approach would be important for monitoring, at molecular level, less known aggregation process of other metabolites occurring under different physicochemical conditions.

2 | Experimental Section

L-tryptophan (purity $\geq 98\%$), thioflavin T, silver nitrate (AgNO_3), sodium citrate, and sodium nitrate (NaNO_3) were purchased from Sigma-Aldrich. Ultrapure water purified by a Millipore Synergy Water Purification System was used for the synthesis of silver nanoparticles (AgNPs) and sample preparations.

2.1 | Amyloid-Like Aggregates Preparation

For the self-assembling experiments, L-tryptophan was dissolved at a concentration of 4.0 mg/mL in ultrapure water. The Trp samples were stored at 38°C in a Stuart Scientific SHT 2D heater and left to self-assemble into amyloid-like aggregates for several days. This temperature was chosen due to its proximity to physiological temperatures, as well as from previous reports of Trp aggregation into amyloid type fibrils in similar conditions [16]. Multiple samples were prepared to ensure the reproducibility of the preparation method.

2.2 | Synthesis of AgNPs

The AgNPs were synthesized by reducing AgNO_3 with sodium citrate in a method established by Lee and Meisel [71]. For that, 18 mg of AgNO_3 was dissolved in 100 mL of water. The resulting solution was heated to boil, at which point 2 mL of 1% sodium citrate in water was added. The resulting suspension was left heating for another 40 min.

2.3 | Static Fluorescence Spectroscopy

The measurements of intrinsic Trp fibrils fluorescence and ThT stain fluorescence were conducted in a Varian Cary Eclipse Fluorescence Spectrophotometer using a 10-mm quartz cuvette, with 5-mm excitation and emission slits and a high detection sensibility. A stock solution of ThT was added to the Trp sample before each measurement, reaching a final concentration of 20 μM . The solution was then stirred and left at room temperature for 15 min to allow interaction with present amyloid fibrils. The excitation wavelength used for the ThT fluorescence was 430 nm. Intrinsic fluorescence of the Trp fibrils was also measured without any dye. In this case, an excitation wavelength of 375 nm was used.

2.4 | Scanning Electron Microscopy (SEM)

A Trp sample was prepared and left to aggregate for 12 days following a normal sample preparation. After that, 60- μL aliquot of the solution was deposited in a Al-Cu alloy stub and left to dry at ambient conditions. The sample was then sputtered with gold for 180 s. The micrographs were obtained using a LEO Electron

Microscopy/Oxford Leo 440i microscope at a constant voltage of 20 kV.

2.5 | Surface-Enhanced Raman Spectroscopy

SERS spectra were recorded using an EZRaman-1-Dual-G by Enwave Optronics Inc. with an excitation wavelength of 785 nm, power of 20 mW, and 10-s acquisition time. Each measure represented the average between 10 acquisitions. To demonstrate the reproducibility of the approach, we have included in Figure S1 the comparison of the spectra of different samples obtained with two different batches of Lee–Meisel colloidal nanoparticles. An automatic baseline correction was made using the software EZRaman Reader V8.2.9 included in the Raman spectrometer. All obtained SERS spectra were normalized using the intensity of the band at 1009 cm^{-1} , whose intensity and position are almost unaffected by the interactions involved in the self-assembling process. Spectra deconvolution using Lorentzian functions was carried out. Sodium nitrate was used as an aggregation agent. At each time point, the samples for SERS were prepared as follows: $\{[50\ \mu\text{L} (\text{Trp}, 4\ \text{mg/mL}) + 50\ \mu\text{L} (\text{NaNO}_3, 0.2\ \text{M})] + 100\ \mu\text{L} (\text{AgNP})\}$. The final concentration of Trp in the measured solution was 4.9 mM.

2.6 | Computational Methods

Full geometry optimization, vibrational wavenumbers and Raman activity for Trp and for a Trp dimer was carried out using density functional theory (DFT) [72]. The initial dimer structural configuration showing simultaneously π -stacking and hydrogen bonding interactions was obtained from the Trp crystal structure [24]. These calculations were performed with the Meta-GGA hybrid functional M06-2X [73–75] and Pople basis set functions, 6-311++G(d,p) [76], which includes diffuse and polarization functions in all atoms. This level of calculation has shown promising results in previous studies of Trp and other aromatic amino acids [77, 78]. To incorporate the effect of the solvent in the geometry and vibrational wavenumbers, the polarizable continuum model (PCM) [79] was used. All calculations were performed with Gaussian 09 software [80]. Figure 1A shows the structure of Trp as well as the atom numbering used here. Table S1 includes the experimental band positions of the SERS spectra of Trp at $t=0$ and $t=12$ days as well as the calculated wavenumber, Raman activity, infrared intensity, and normal mode description of Trp. The band assignment was conducted considering previous works [81–83]. The calculated wavenumbers and normal modes the Trp dimer and their correspondence to Trp monomer vibrational modes are present in Table S2. The coordinates of the optimized Trp and Trp dimer structures are also available in Tables S3 and S4, respectively.

3 | Results and Discussion

The structural morphology of the final metabolite self-assemblies, including those of Trp, have already been well studied using techniques such as transmission electron microscopy and SEM and fluorescence lifetime imaging microscopy [6, 8–12, 14, 16, 17]. Therefore, to detect the presence of amyloid-like

fibrils in solution during kinetics we have limited our study to the use of intrinsic fibril fluorescence and extrinsic fluorescence probe. There is sufficient evidence that both methods can detect the fibril formation [6, 8, 10, 11, 15–17]. To characterize the final Trp supramolecular structures, we have also carried out SEM measurements (Figure 2A–C). The observed morphology is similar to those previously obtained by other studies [12, 16].

Figure 2 D and E show the ThT and intrinsic fluorescence of Trp at different time points. No appreciable changes in the ThT fluorescence were observed in 1 day (see inset). After that, there is an increase in the signal with time suggesting the formation of amyloid-like structures [10, 16]. Wu et al. used MD simulations to

study the binding of ThT to peptide self-assembly that mimics a β -sheet. They found that the dye binds specifically to aromatic-hydrophobic grooves in the amyloid fibril surfaces [84]. This and other studies suggest that ThT may have affinity for hydrophobic regions in the Trp self-assembled structure [84, 85]. This interpretation is also supported by the study of Harel et al. where in the crystal structure of *Torpedo californica* acetylcholinesterase, ThT was observed to be surrounded by the side chains of several aromatic residues [86]. Moreover, the intrinsic fluorescence also starts increasing after 1 day upon initiating the kinetics (see Figure 2D, inset). In the case of amino acids self-assembling, the intrinsic fluorescence may reflect the presence of layers formed by hydrogen bonding interactions in a β -like sheet structure [15, 19].

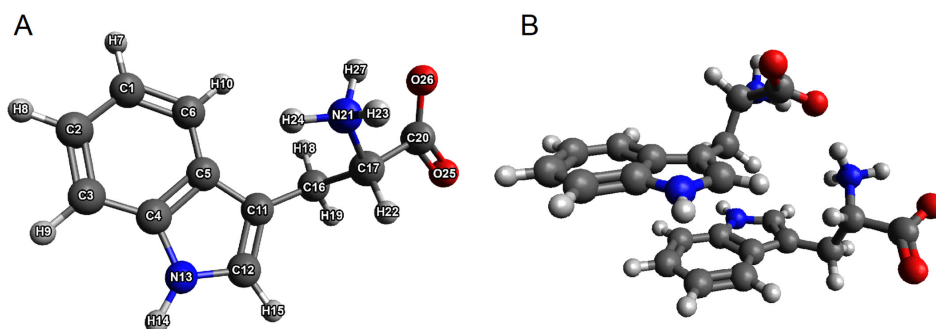


FIGURE 1 | (A) Optimized L-tryptophan structure with atoms numbering. (B) Optimized tryptophan dimer.

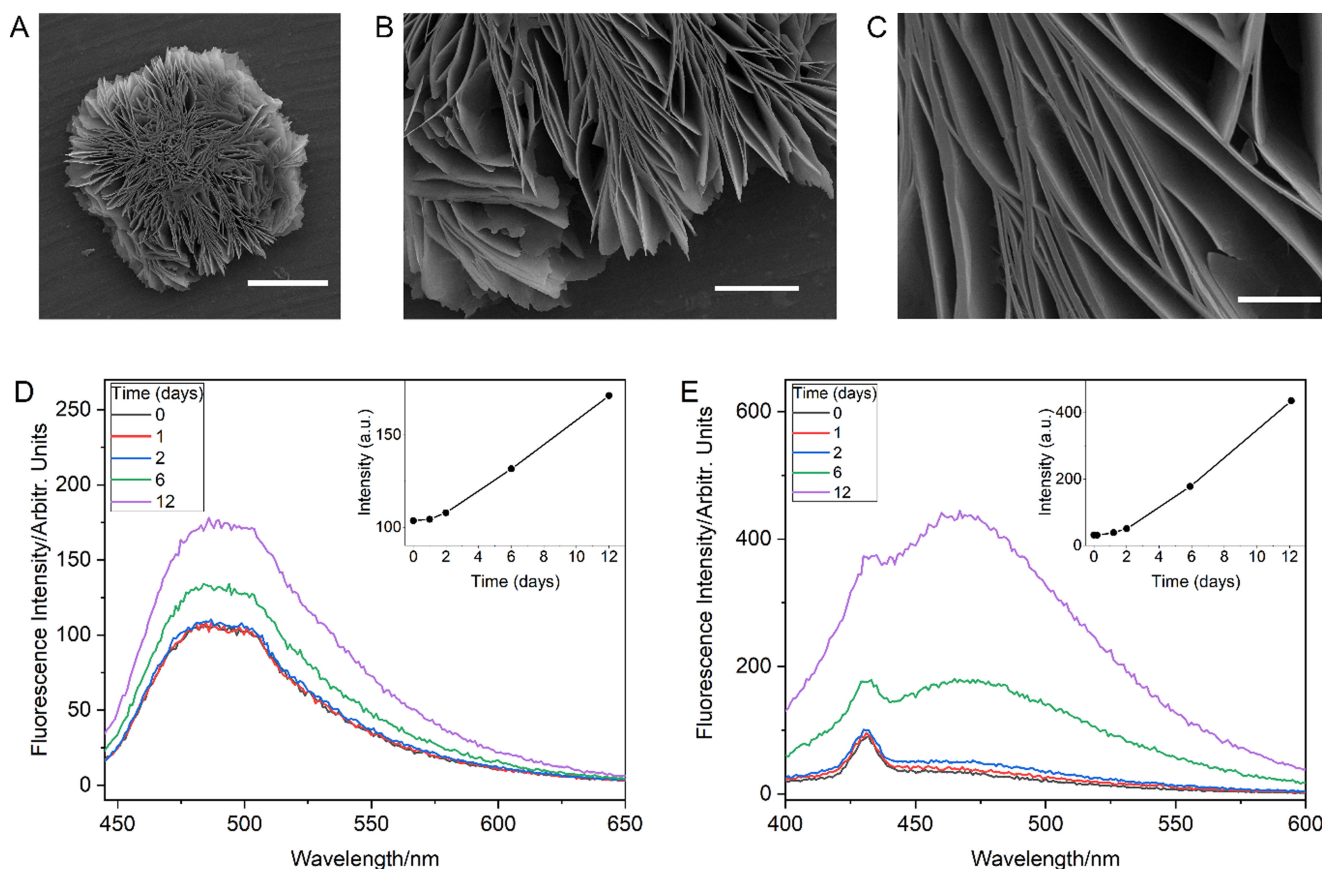


FIGURE 2 | (A–C) SEM micrographs of Trp supramolecular structures with different resolutions. Scale bars are (A) 100 μ m, (B) 30 μ m, and (C) 6 μ m. (D) ThT fluorescence in the presence of Trp in multiple time points. Excitation wavelength was 430 nm. Inset: Emission intensity at a wavelength of 490 nm as a function of time. (E) Intrinsic fluorescence of Trp fibrils in multiple points in time. The smaller peak at around 430 nm corresponds to a Raman signal of water. Excitation wavelength was 375 nm. Inset: Emission intensity at a wavelength of 470 nm.

Based on the literature we can give a possible explanation of the behavior of the fluorescence data during Trp self-assembling. The observation of intrinsic fluorescence indicates that the structures initially formed by Trp may have single ladder-like layer or pore-like tube forms [10, 12, 19, 23, 24]. Multiple of these structures may form higher ordered aggregates with regions of high hydrophobicity where ThT can be inserted, increasing its fluorescence signal.

To get more information about the self-assembling process, we have recorded the SERS spectra of Trp as a function of time. It is important to note that the SERS signal has a contribution from molecules placed within a few nanometers from the metal surface in dependence of the nanoparticle size [87]. Thus, considering the size of Trp ($\sim 8 \text{ \AA}$) it can be inferred that the nanoplasmonic enhancement may occur for molecules placed in both hydrophobic and hydrophilic regions, as observed in the crystal structure obtained by Görbitz et al. [24] Figure 3 shows the changes in the SERS spectra as a function of time for several days. The spectrum at $t=0$ days corresponds to Trp in monomeric form and the spectral profile is similar to those from normal Raman and UVRF with contributions mainly from the indole in-plane vibrations [68, 81, 88–91]. Very weak bands assigned to out-of-plane vibrations are also observed in SERS. From the SERS selection rules, this result indicates that the indole ring may be placed approximately perpendicular to the AgNP surface [92–94]. The spectrum at 12 days shows several differences with respect to that of the monomer and, from the fluorescence results, it can be assigned to the higher ordered self-assembled aggregates of Trp.

The spectrum at 12 days shows intense bands at 1638 and 1039 cm^{-1} , which are not present in the spectrum of the monomer at $t=0$ days. To the best of our knowledge, the presence of the intense band at 1638 cm^{-1} is anomalous because it has not been previously reported in the Raman spectrum of Trp. These bands start appearing after 1 day and, as shown in Figure 4, increase in intensity with a similar trend to the intrinsic and extrinsic fluorescence signals. As shown in Figure 5, the 1638 cm^{-1}

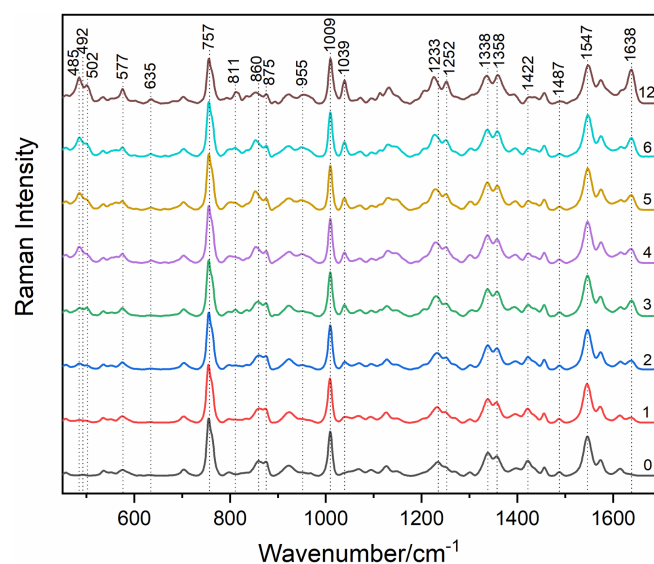


FIGURE 3 | SERS spectra of Trp at various moments in time along the self-assembly process. Time of recording each spectrum is indicated in days, at the right. Dotted lines mark the position of relevant bands, in cm^{-1} .

band is assigned to a combination of carbonyl stretching (COO^-) and NH_3^+ scissoring. The band at 1039 cm^{-1} is assigned mainly to the main chain movements: NH_3^+ rocking, $+\text{H}_{18}-\text{C}_{16}-\text{H}_{19}$ twisting and $+\text{N}_{21}-\text{C}_{17}$ stretching. The band at 1422 cm^{-1} , with vibrational contribution from these atomic groups, also changes in intensity with time (see Figure 4). From previous studies, we can assume that the carboxylate and amine groups of Trp are in the interior of the self-assembled structures [10, 12, 19, 23, 24],

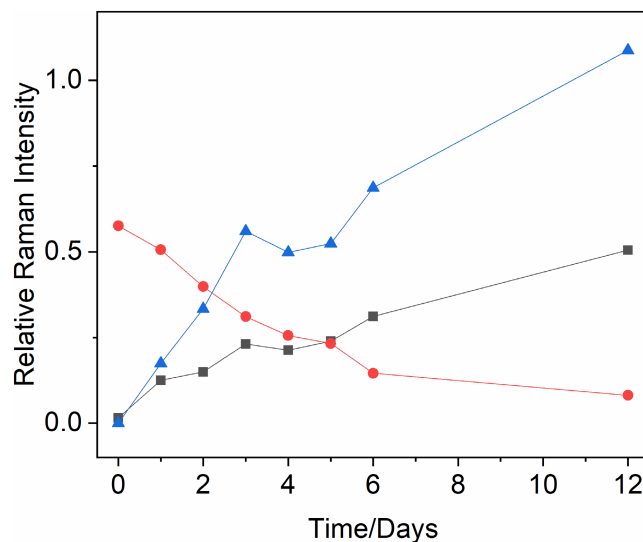


FIGURE 4 | Time evolution of the relative intensities $I/I_{1039 \text{ cm}^{-1}}$ of the bands 1039 (square), 1422 (circle), and 1638 cm^{-1} (triangle).

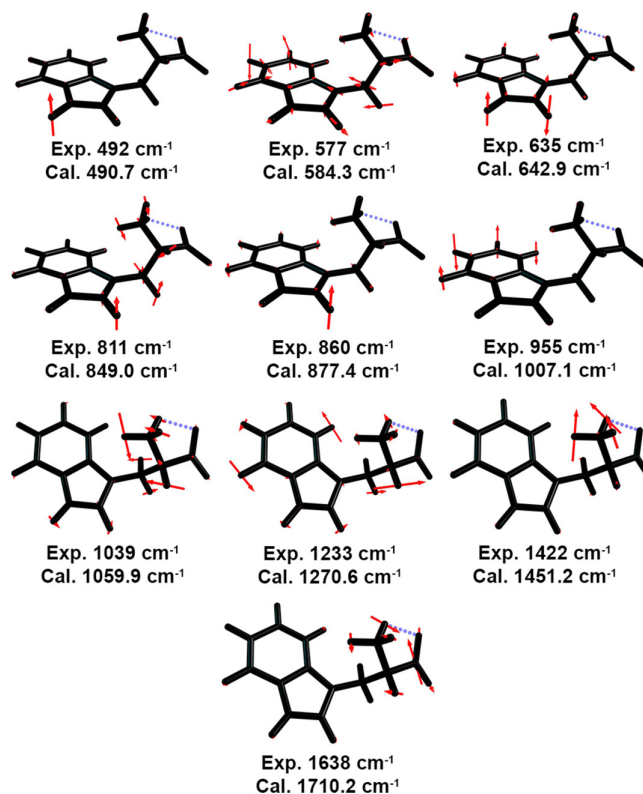


FIGURE 5 | Ten normal modes of Trp with calculated and experimental wavenumbers. Red arrows indicate the normal modes displacement vectors.

meaning that the adsorption on the nanoparticle surface may occur through the indole rings. Hence, the increase in the intensity of these bands does not seem to be due to direct interaction of these atomic groups with the AgNP surface. The changes can be correlated with the interaction between carboxylate and amine groups contributing to the formation of hydrogen bonding mediated supramolecular β -strand-like structures, as also detected by the intrinsic fluorescence [19]: Interestingly, both set of signals (intensity of the 1638 and 1039 cm^{-1} Raman bands and intrinsic fluorescence) exhibit a similar time evolution. Another effect that could potentially influence the intensity of these peaks is the difference in the orientation of the COO^- and NH_3^+ groups with respect to the metal surface in the aggregated structures [92–94]. From the available crystal structure, it can be suggested that the COO^- and NH_3^+ of different Trp molecules in the self-assembled structure adopt different conformational configurations with respect to the nanoparticle surface. Considering the ensemble average of the conformations of all Trp in the ordered structure, this effect may not have substantial contribution to the intensity enhancement. Therefore, the presence of these bands is either directly or indirectly related to the formation of multiple hydrogen bonds between the carboxylate and amine groups during self-assembling. Thus, the bands at 1638, 1422, and 1039 cm^{-1} can be considered as characteristic SERS markers of the Trp self-assembled structures in water.

After 1 day, the initially weak single band at 492 cm^{-1} in the monomer splits into two bands observed at 485 and 502 cm^{-1} (see Figure 3). The intensity of these bands also increases as a function of time during the self-assembly process as shown in Figure 6A. The band at 492 cm^{-1} has contribution only from $\text{N}_{13}\text{H}_{14}$ out-of-plane bending from the pyrrole ring and its position would be affected by hydrogen bonding interactions involving the $\text{N}_{13}\text{H}_{14}$ group as a donor (see Figure 5). Using NMR, Bera et al. showed that with the increase in Trp concentration there are variations in the chemical shifts of H_{14} and H_{15} atoms [12]. It was suggested that this occurs due to the involvement of the NH group of indole ring in hydrogen bonding interactions [12]. However, after 1 day, no appreciable changes can be observed in the position of the Trp Raman markers well-known to be sensitive to hydrogen bonding, such as the bands observed here at 875

and 1487 cm^{-1} [65, 66, 68, 88]. Thus, the splitting of the 492 cm^{-1} peak must be caused by effects other than hydrogen bonding interactions. In the SERS spectrum of the monomer there is a band at 860 cm^{-1} , which downshifts and becomes broader with time (see Figure 6B). This peak is assigned mainly to $\text{C}_{12}\text{H}_{15}$ out-of-plane bending from the pyrrole ring (see Figure 5). These results may indicate that in the self-assembled structure, the NH and CH groups of the pyrrole ring of different Trps are exposed to different local environments. This interpretation is supported by the crystal structure and MD simulations, where the indole ring of different Trps can adopt diverse structural configurations due to the presence of π - π and CH- π interactions [12, 23, 24]. For example, it is possible to find π - π parallel displaced interactions between indole rings and CH- π interactions in which hydrogens of benzene, pyrrole or both can act as donors. Previous Raman studies also suggest that the out-of-plane vibrations of the NH and CH groups may be affected by π - π and CH- π interactions involving the electron density of the pyrrole ring [40, 57, 60, 70]. Thus, the changes in the SERS spectra indicates that upon 1 day of initiating the self-assembling clusters of Trps joined by hydrogen bonding between carboxylate and amino groups also start forming π - π and CH- π interactions.

To get more insights about self-assembled structures, we analyzed other Raman bands sensitive to interactions involving the electron density of the indole ring. Interestingly, the two components of the called Fermi doublet bands (~ 1340 and ~ 1360 cm^{-1}) of Trp also change their positions as a function of time (see Figure 7A,B). In the protein barstar, the lower and higher wavenumber bands of the Trp53 Fermi doublet shift -9 and $+7$ cm^{-1} , respectively, in comparison to those of N-acetyl-tryptophanamide in water [32, 57]. This behavior of the Fermi doublet has also been previously reported in only a few other cases [40, 55, 63, 70]. Schlamadinger et al. observed shifts in the Fermi doublet of the TrpZip2 peptide, and it was related to the contribution of Trp to π - π interactions [70]. The NMR structure of TrpZip2 shows the possibility of Trps involvement in π - π and CH- π interactions [70, 95]. Sanchez et al. also detected similar changes in the positions of the Fermi doublet components of Trp15 in a mutant of the outer membrane protein OmpA during refolding in the presence of lipid vesicles

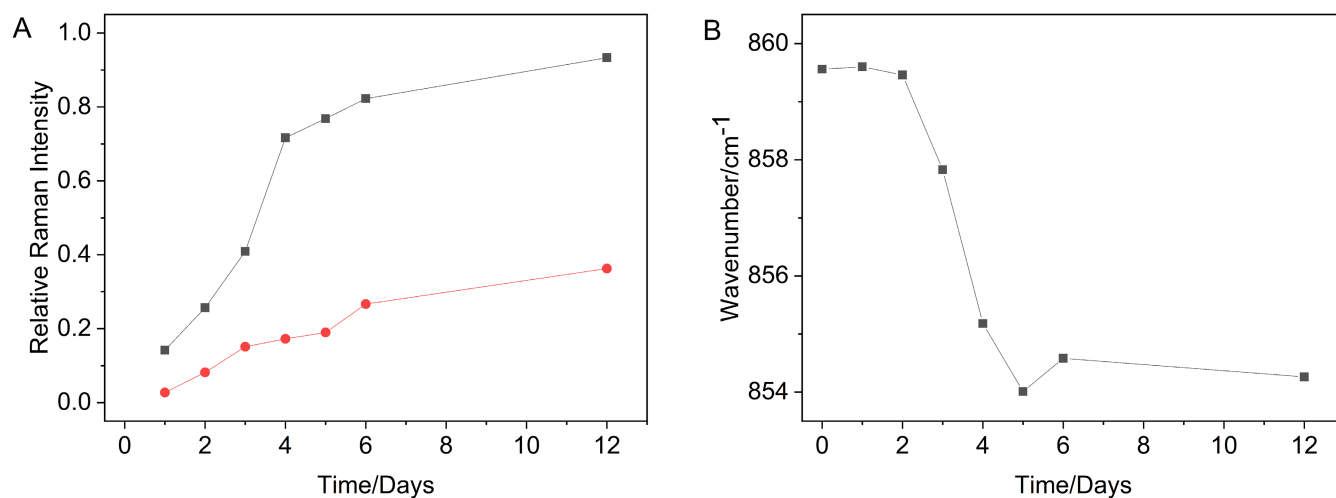


FIGURE 6 | (A) Time evolution of the relative intensities $I/I_{1009\text{ cm}^{-1}}$ of the bands 485 (square) and 502 cm^{-1} (circle), (B) temporal evolution of position of the band 860 cm^{-1} .

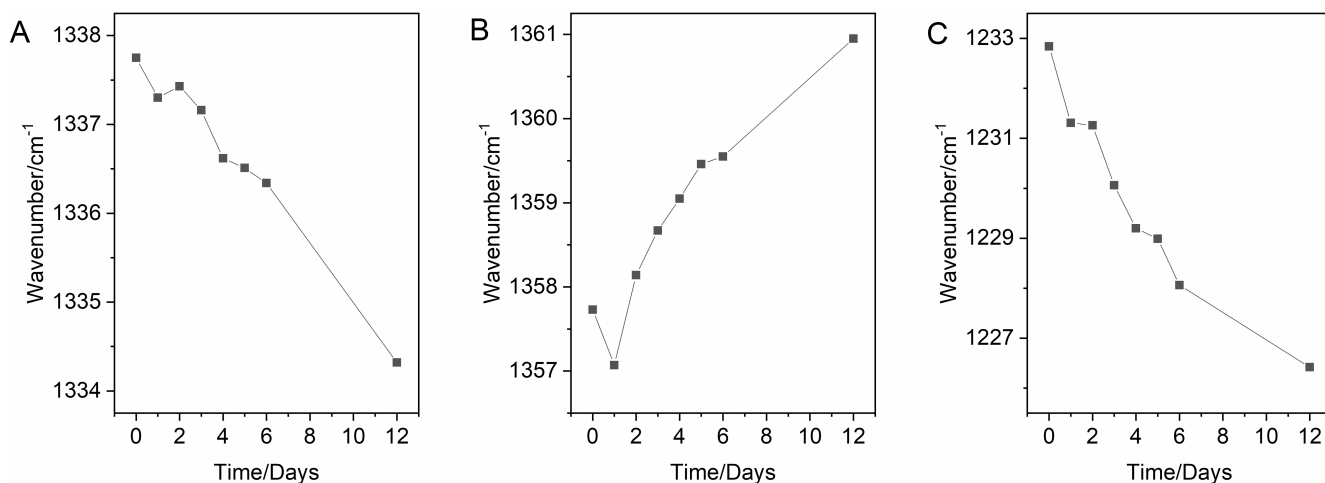


FIGURE 7 | Temporal evolution of position of the bands (A) 1338, (B) 1358, and (C) 1233 cm^{-1} .

[40]. The shifts were related to the formation of cation- π interactions with the lipid headgroup during folding. As shown in Figure 7C, during the self-assembling process the band at 1233 cm^{-1} in the monomer also downshifts to 1226 cm^{-1} in the self-assembled structure. Similar variations have been previously reported with UVRR for the residues Trp53, Trp182, and Trp38 in barstar, bacteriorhodopsin, and filamentous virus Pf3, respectively [32, 55, 57, 63]. In barstar, the Trp53 residue is involved in CH- π interactions with Phe56 in an edge-to-face configuration and with a methyl group of Ile5 from the other side of the indole ring [32, 57]. The interaction of a methyl group of retinal with the side chain of Trp182 in bacteriorhodopsin also induces a shift in this band [55]. In the filamentous virus Pf3, Trp38 is in a favorable cation- π interaction with Arg37 and Lys40 [63]. Thus, the observed changes in the positions of the 1233 cm^{-1} and the Fermi doublet bands during the self-assembling process of Trp are direct evidence of the perturbation of the indole π -electron system due to π -stacking. Surprisingly, these changes have similarities with those observed for Trp53 during the refolding of the protein barstar [32].

To determine the effect of interactions involving the indole π -electron system on the Raman spectrum of Trp, we have carried out DFT calculations using a dimer forming a π - π interaction. As shown in Figure 1B and Figure S2, the optimized structure of the Trp-Trp dimer corresponds to a parallel displaced configuration of the indole rings. The planes of the rings are separated by 3.3 Å and the distance between the closest benzene and pyrrole ring is 3.5 Å. The displacement angle Θ between both rings is 20.33°. The structural characteristics of the optimized dimer have an excellent match with what has been reported for π - π interactions from calculations of model system such as 3-methylindole dimers, indole-benzene and indole-imidazole [96–99]. Databanks analysis of π - π interactions also shows, in similar systems such as indole-indole in crystals or aromatic amino acids in proteins, ring distances and Θ angle distributions that are in excellent agreement with the obtained values for the Trp-Trp dimer [100–102]. To the best of our knowledge, this is the first computationally reported molecular dimer of Trp simultaneously stabilized by both π - π and hydrogen bonding interactions in a single optimized geometry. In a previous study,

the optimized structure of a Trp dimer was reported but the only interaction considered was hydrogen bonding between the main chains [103].

The obtained vibrational modes of the dimer were compared with those of the monomer, as seen in Table S2. Interestingly, the difference in the wavenumber of some modes of the monomer and the dimer match well to what was experimentally observed. For example, the $\text{N}_{13}\text{H}_{14}$ out-of-plane bending from the pyrrole ring associated to the band at 492 cm^{-1} , calculated at 490.7 cm^{-1} in the monomer, is present in the dimer in five vibrational modes: four downshifted at 462.1, 462.7, 464.8, and 468.7 cm^{-1} and one upshifted at 505.7 cm^{-1} (see Figure 8A–E). This result correlates well with the splitting of the 492 cm^{-1} band in the SERS spectra. The band at 860 cm^{-1} calculated at 877.4 cm^{-1} in the monomer is predicted to be downshifted at 863.3 and 871.1 cm^{-1} in the dimer (see Figure 8F,G). Additionally, the shift of the 1233 cm^{-1} , calculated in the monomer at 1270.6 cm^{-1} , is also observed in the calculated dimer at 1256.8 cm^{-1} (see Figure 8H). This is further evidence that the changes in the SERS spectra are indicators of π -stacking interactions involving the indole ring.

Previous UVRR studies have shown that interactions involving the indole π -electron system may decrease the relative intensity of the band at $\sim 760 \text{ cm}^{-1}$ [40, 53, 57, 60]. A slight change in the relative intensity of the band at 757 cm^{-1} during self-assembling of Trp is also observed in SERS. The excitation wavelength used here is far from the UV region, indicating that the intensity change observed in SERS is not related to electronic resonance of the molecule but to other effects. Because this band is assigned to indole ring breathing vibration, the presence of π - π and CH- π interactions in the self-assembled structure may also have direct influence in its intensity.

During the self-assembly process, some hydrogen out-of-plane vibrations of the indole ring, which were initially weak or absent in the SERS spectrum of the monomer, increase their intensity as function of time: 955, 811, 635, 577, 485, and 502 cm^{-1} (see Figures 3, 5, and 6). UVRR studies suggest that in the presence of interactions involving the indole

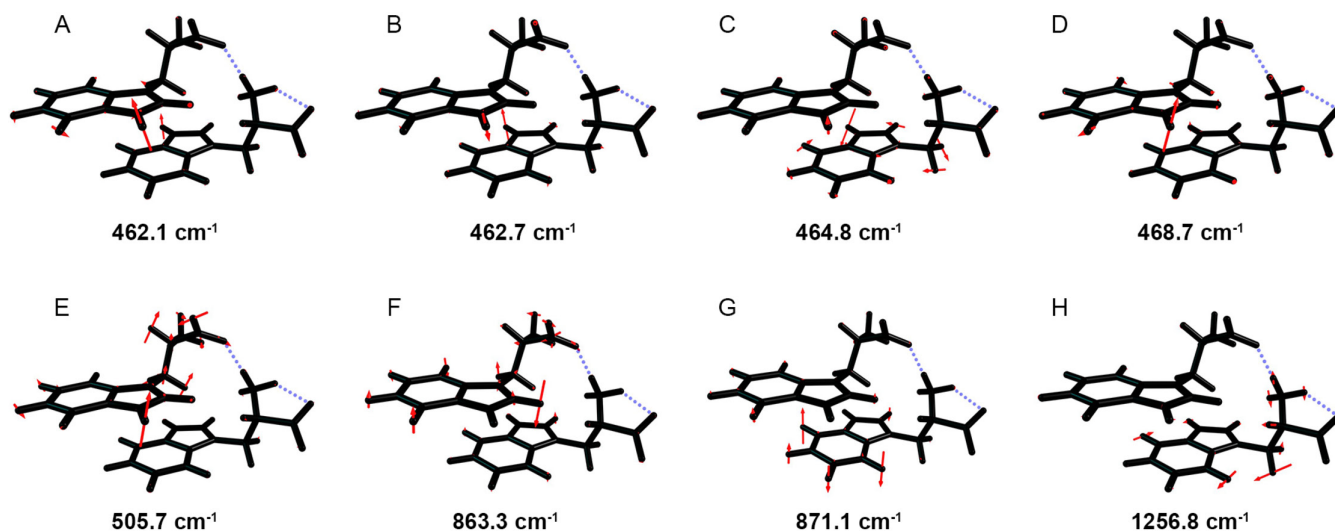


FIGURE 8 | Eight calculated wavenumbers and normal modes of Trp dimer. Red arrows indicate the normal modes displacement vectors.

π -electron density, the Raman intensity of some hydrogen out-of-plane vibrations can be enhanced [32, 40, 53, 57, 60]. In SERS, the intensity analysis is more complex as it is necessary to consider the orientation of the adsorbed molecules on the nanoparticle surface. Due to their previously suggested morphology, it is expected that the self-assembled amyloid-like structures of Trp are adsorbed such that the axis of the fibers is parallel to the nanoparticle surface with the indole ring close to the surface. According to the SERS selection rules, the presence of out-of-plane vibration bands indicates that the ring is tilted with respect to the nanoparticle surface [92–94]. In the spectrum of the monomer, only few of these bands are present and they are weak in intensity indicating that the indole ring may adopt a quasi-perpendicular orientation on the surface. During self-assembling, their intensity increases relative to those of other in-plane vibrations, implying that the indole ring adopts a more tilted configuration with respect to the nanoparticle surface. This result agrees with the obtained crystal structure and MD simulations of Trp, which show that the indole ring is kept tilted with respect to the axis of the β -strand-like structures [12, 24]. From our data, it is not possible to know whether the intensity changes of these bands occur due to the perturbation of the π -electron density, due to the reorientation of the indole ring with respect to the surface or both effects. Future studies are required to determine the mechanisms of enhancement of these bands, which may be carried out by using UV resonance Raman spectroscopy.

The relative intensity of the Fermi doublet ($R_{W7} = I_{-1360\text{ cm}^{-1}}/I_{-1340\text{ cm}^{-1}}$) is a commonly used hydrophobicity Raman marker. From normal Raman and URR studies, it has been found that the ratio R_{W7} increases when the indole ring is in a more hydrophobic environment [65–67, 69]. The R_{W7} of the 4 day spectrum does not show a significant difference in comparison with the spectrum of the monomer (see Figure 3) [65–69]. However, after that, the R_{W7} value slightly increases as a function of time during self-assembling. The crystal structure of Trp and the MD simulations of self-assembled aggregates show that the indole ring is in a hydrophobic environment [12, 23, 24]. Thus, the changes of the R_{W7} values in SERS, also correlate well with the indole ring being

in a more hydrophobic environment during self-assembling as also observed from the ThT fluorescence data [84, 85]. These results also strengthen the idea that hydrophobicity, together with hydrogen bonding and π -stacking interactions, plays an important role in the self-assembling of this aromatic amino acid.

4 | Conclusion

In this work, we have shown that SERS can be a useful method to monitor the kinetics of the self-assembling of metabolites in a label-free manner. The SERS spectrum of Trp was sensible to several intermolecular interactions that play important roles in the self-assembling process. The time dependent evolution observed in SERS was consistent with the increase in the amyloid-like fibril fluorescence. From the detailed analysis of the SERS spectra and from previous studies [10, 12, 19, 23, 24], it is possible to describe the following steps in the self-assembly process. Upon 1 day of initiating the reaction, the bands at 1637 and 1039 cm^{-1} appear in the spectrum, indicating the formation of hydrogen bonding interaction between the carboxylate and amino groups of the main chain, probably forming dimers, tetramers, or other high-ordered structures [10, 12, 18, 19, 22, 24]. After 1 day, the splitting of the band at 492 cm^{-1} occurs accompanied by a shift in the components of Fermi doublet and the band at 1233 cm^{-1} . At this time, the formation of π - π and CH- π interactions may occur, inducing the formation of small clusters of Trp. This is followed by an increase in the hydrophobicity of the local environment of indole rings as found from the R_{W7} Fermi doublet ratio. The continuous shifts of few bands as function of time suggest that due to π - π and CH- π interactions the supramolecular structures may become more packed.

The SERS based methodology presented here has the advantage of being simple, providing direct, experimental information about intermolecular interactions that are relevant in the aggregation process and allowing for a kinetics study with sufficient temporal resolution. This methodology can be useful in obtaining new insights about the aggregation processes of other metabolites under different physicochemical conditions.

Author Contributions

The manuscript was written through contributions of all authors. All authors have given approval to the final version of the manuscript.

Acknowledgments

This work was supported by grant #2021/01593-1, São Paulo Research Foundation (FAPESP). G.C.C. was supported by a CNPq fellowship. M.T.L. and M.A.R. are recipients of CNPq research fellowships. Research developed with the help of HPC resources made available by the Technology Superintendence of Information from the University of São Paulo. SEM measurements made with help from the laboratory LabMev-IGC-USP. The Article Processing Charge for the publication of this research was funded by the Coordenação de Aperfeiçoamento de Pessoal de Nível Superior - Brasil (CAPES) (ROR identifier: 00x0ma614).

Conflicts of Interest

The authors declare no conflicts of interest.

Data Availability Statement

The data that support the findings of this study are available from the corresponding author upon reasonable request.

References

1. T. P. J. Knowles, M. Vendruscolo, and C. M. Dobson, "The Amyloid State and Its Association With Protein Misfolding Diseases," *Nature Reviews. Molecular Cell Biology* 15 (2014): 384–396.
2. F. Chiti and C. M. Dobson, "Protein Misfolding, Functional Amyloid, and Human Disease," *Annual Review of Biochemistry* 75 (2006): 333–366.
3. H. Levine, "Thioflavine T Interaction With Synthetic Alzheimer's Disease β -Amyloid Peptides: Detection of Amyloid Aggregation in Solution," *Protein Science* 2 (1993): 404–410.
4. H. Naiki, K. Higuchi, M. Hosokawa, and T. Takeda, "Fluorometric Determination of Amyloid Fibrils In Vitro Using the Fluorescent Dye, Thioflavine T," *Analytical Biochemistry* 177 (1989): 244–249.
5. D. Pinotsi, A. K. Buell, C. M. Dobson, G. S. Kaminski Schierle, and C. F. Kaminski, "A Label-Free, Quantitative Assay of Amyloid Fibril Growth Based on Intrinsic Fluorescence," *Chembiochem* 14 (2013): 846–850.
6. Z. A. Arnon, T. Kreiser, B. Yakimov, et al., "On-Off Transition and Ultrafast Decay of Amino Acid Luminescence Driven by Modulation of Supramolecular Packing," *iScience* 24 (2021): 102695.
7. N. Balasco, C. Diaferia, E. Rosa, et al., "A Comprehensive Analysis of the Intrinsic Visible Fluorescence Emitted by Peptide/Protein Amyloid-like Assemblies," *International Journal of Molecular Sciences* 24 (2023): 8372.
8. L. Adler-Abramovich, L. Vaks, O. Carny, et al., "Phenylalanine Assembly Into Toxic Fibrils Suggests Amyloid Etiology in Phenylketonuria," *Nature Chemical Biology* 8 (2012): 701–706.
9. D. Banik, S. Kundu, P. Banerjee, R. Dutta, and N. Sarkar, "Investigation of Fibril Forming Mechanisms of L-Phenylalanine and L-Tyrosine: Microscopic Insight Toward Phenylketonuria and Tyrosinemia Type II," *Journal of Physical Chemistry B* 121 (2017): 1533–1543.
10. S. Shaham-Niv, P. Rehak, L. Vuković, L. Adler-Abramovich, P. Král, and E. Gazit, "Formation of Apoptosis-Inducing Amyloid Fibrils by Tryptophan," *Israel Journal of Chemistry* 57 (2017): 729–737.
11. S. Shaham-Niv, L. Adler-Abramovich, L. Schnaider, and E. Gazit, "Extension of the Generic Amyloid Hypothesis to Nonproteinaceous Metabolite Assemblies," *Science Advances* 1 (2015): 7.
12. S. Bera, B. Xue, P. Rehak, et al., "Self-Assembly of Aromatic Amino Acid Enantiomers Into Supramolecular Materials of High Rigidity," *ACS Nano* 14 (2020): 1694–1706.
13. R. Perkins and V. Vaida, "Phenylalanine Increases Membrane Permeability," *Journal of the American Chemical Society* 139 (2017): 14388–14391.
14. S. Perween, B. Chandanshive, H. C. Kotamarthi, and D. Khushalani, "Single Amino Acid Based Self-Assembled Structure," *Soft Matter* 9 (2013): 10141.
15. S. Shaham-Niv, Z. A. Arnon, D. Sade, et al., "Intrinsic Fluorescence of Metabolite Amyloids Allows Label-Free Monitoring of Their Formation and Dynamics in Live Cells," *Angewandte Chemie, International Edition* 57 (2018): 12444–12447.
16. K. P. Prajapati, B. G. Anand, M. Ansari, A. B. Tikku, and K. Kar, "Tryptophan Self-Assembly Yields Cytotoxic Nanofibers Containing Amyloid-Mimicking and Cross-Seeding Competent Conformers," *Nanoscale* 14 (2022): 43–16285.
17. P. Banerjee, A. Pyne, and N. Sarkar, "Understanding the Self-Assembling Behavior of Biological Building Block Molecules: A Spectroscopic and Microscopic Approach," *Journal of Physical Chemistry B* 124 (2020): 2065–2080.
18. T. D. Do, W. M. Kincannon, and M. T. Bowers, "Phenylalanine Oligomers and Fibrils: The Mechanism of Assembly and the Importance of Tetramers and Counterions," *Journal of the American Chemical Society* 137 (2015): 10080–10083.
19. S. Bera, S. Mondal, S. Rencus-Lazar, and E. Gazit, "Organization of Amino Acids into Layered Supramolecular Secondary Structures," *Accounts of Chemical Research* 51 (2018): 2187–2197.
20. E. Mossou, S. C. M. Teixeira, E. P. Mitchell, et al., "The Self-Assembling Zwitterionic Form of L-Phenylalanine at Neutral pH," *Acta Crystallographica Section C* 70 (2014): 326–331.
21. D. G. Babar and S. Sarkar, "Self-Assembled Nanotubes From Single Fluorescent Amino Acid," *Applied Nanoscience* 7 (2017): 101–107.
22. H. W. German, S. Uyaver, and U. H. E. Hansmann, "Self-Assembly of Phenylalanine-Based Molecules," *Journal of Physical Chemistry. A* 119 (2015): 1609–1615.
23. S. Uyaver, H. W. Hernandez, and M. Gokhan Habiboglu, "Self-Assembly of Aromatic Amino Acids: A Molecular Dynamics Study," *Physical Chemistry Chemical Physics* 20 (2018): 30525–30536.
24. C. H. Görbitz, K. W. Törnroos, and G. M. Day, "Single-Crystal Investigation of L-Tryptophan With $Z' = 16$," *Acta Crystallographica. Section B* 68 (2012): 549–557.
25. S. Olsztyńska-Janus and M. Komorowska, "Conformational Changes of L-Phenylalanine Induced by Near Infrared Radiation. ATR-FTIR Studies," *Structural Chemistry* 23 (2012): 1399–1407.
26. D. Tomar, S. Chaudhary, and K. C. Jena, "Self-Assembly of L-Phenylalanine Amino Acid: Electrostatic Induced Hindrance of Fibril Formation," *RSC Advances* 9 (2019): 12596–12605.
27. M. Brandl, M. S. Weiss, A. Jabs, J. Sühnel, and R. Hilgenfeld, "C-H... π -Interactions in Proteins," *Journal of Molecular Biology* 307 (2001): 357–377.
28. M. J. Plevin, D. L. Bryce, and J. Boisbouvier, "Direct Detection of CH/ π Interactions in Proteins," *Nature Chemistry* 2 (2010): 466–471.
29. J. Shao, B. P. Kuiper, A.-M. W. H. Thunnissen, et al., "The Role of Tryptophan in π Interactions in Proteins: An Experimental Approach," *Journal of the American Chemical Society* 144 (2022): 13815–13822.

30. S. K. Burley and G. A. Petsko, "Aromatic-Aromatic Interaction: A Mechanism of Protein Structure Stabilization," *Science* 229 (1985): 23–28.
31. N. Kuhar, S. Sil, and S. Umapathy, "Potential of Raman Spectroscopic Techniques to Study Proteins," *Spectrochimica Acta Part A: Molecular Spectroscopy* 258 (2021): 119712.
32. E. A. Milán-Garcés, P. Thaore, J. B. Udgaonkar, and M. Puranik, "Formation of a CH– π Contact in the Core of Native Barstar during Folding," *Journal of Physical Chemistry B* 119 (2015): 2928–2932.
33. G. Balakrishnan, C. L. Weeks, M. Ibrahim, A. V. Soldatova, and T. G. Spiro, "Protein Dynamics From Time Resolved UV Raman Spectroscopy," *Current Opinion in Structural Biology* 18 (2008): 623–629.
34. Z. Chi and S. A. Asher, "UV Raman Determination of the Environment and Solvent Exposure of Tyr and Trp Residues," *Journal of Physical Chemistry B* 102 (1998): 9595–9602.
35. Z. Ahmed, I. A. Beta, A. V. Mikhonin, and S. A. Asher, "UV–Resonance Raman Thermal Unfolding Study of Trp-Cage Shows That It Is Not a Simple Two-State Miniprotein," *Journal of the American Chemical Society* 127 (2005): 10943–10950.
36. S. Takahashi, S.-R. Yeh, T. K. Das, C.-K. Chan, D. S. Gottfried, and D. L. Rousseau, "Folding of Cytochrome C Initiated by Submillisecond Mixing," *Nature Structural & Molecular Biology* 4 (1997): 44–50.
37. Z. Chi and S. A. Asher, "Ultraviolet Resonance Raman Examination of Horse Apomyoglobin Acid Unfolding Intermediates," *Biochemistry* 38 (1999): 8196–8203.
38. C.-Y. Huang, G. Balakrishnan, and T. G. Spiro, "Early Events in Apomyoglobin Unfolding Probed by Laser T-Jump/UV Resonance Raman Spectroscopy," *Biochemistry* 44 (2005): 15734–15742.
39. I. K. Lednev, A. S. Karnoup, M. C. Sparrow, and S. A. Asher, " α -Helix Peptide Folding and Unfolding Activation Barriers: A Nanosecond UV Resonance Raman Study," *Journal of the American Chemical Society* 121 (1999): 8074–8086.
40. K. M. Sanchez, G. Kang, B. Wu, and J. E. Kim, "Tryptophan-Lipid Interactions in Membrane Protein Folding Probed by Ultraviolet Resonance Raman and Fluorescence Spectroscopy," *Biophysical Journal* 100 (2011): 2121–2130.
41. G. Ramachandran, E. A. Milán-Garcés, J. B. Udgaonkar, and M. Puranik, "Resonance Raman Spectroscopic Measurements Delineate the Structural Changes That Occur during Tau Fibril Formation," *Biochemistry* 53 (2014): 6550–6565.
42. D. Kurouski, R. P. Van Duyne, and I. K. Lednev, "Exploring the Structure and Formation Mechanism of Amyloid Fibrils by Raman Spectroscopy: A Review," *Analyst* 140 (2015): 4967–4980.
43. I. Lednev, V. Shashilov, and M. Xu, "Ultraviolet Raman Spectroscopy is Uniquely Suitable for Studying Amyloid Diseases," *Current Science* 97, no. 2 (2009): 180–185.
44. S. Mukhopadhyay, "The Dynamism of Intrinsically Disordered Proteins: Binding-Induced Folding, Amyloid Formation, and Phase Separation," *Journal of Physical Chemistry B* 124 (2020): 11541–11560.
45. A. Garcia-Leis and S. Sanchez-Cortes, "Label-Free Detection and Self-Aggregation of Amyloid β -Peptides Based on Plasmonic Effects Induced by Ag Nanoparticles: Implications in Alzheimer's Disease Diagnosis," *ACS Applied Nano Materials* 4 (2021): 3565–3575.
46. S. Bonhommeau, G. S. Cooney, and Y. Huang, "Nanoscale Chemical Characterization of Biomolecules Using Tip-Enhanced Raman Spectroscopy," *Chemical Society Reviews* 51 (2022): 2416–2430.
47. A. K. Dhillon, A. Sharma, V. Yadav, et al., *Wiley Interdisciplinary Reviews: Nanomedicine and Nanobiotechnology* 16, no. 1 (2024): e1917.
48. G. S. Cooney, D. Talaga, V. Ury-Thiery, et al., "Chemical Imaging of RNA-Tau Amyloid Fibrils at the Nanoscale Using Tip-Enhanced Raman Spectroscopy," *Angewandte Chemie, International Edition* 62 (2023): 50.
49. D. Bhowmik, K. R. Mote, C. M. MacLaughlin, et al., "Cell-Membrane-Mimicking Lipid-Coated Nanoparticles Confer Raman Enhancement to Membrane Proteins and Reveal Membrane-Attached Amyloid- β Conformation," *ACS Nano* 9 (2015): 9070–9077.
50. K. Kneipp, Y. Wang, H. Kneipp, et al., "Single Molecule Detection Using Surface-Enhanced Raman Scattering (SERS)," *Physical Review Letters* 78 (1997): 1667–1670.
51. S. Nie and S. R. Emory, "Probing Single Molecules and Single Nanoparticles by Surface-Enhanced Raman Scattering," *Science* 275 (1997): 1102–1106.
52. A. Campion and P. Kambhampati, "Surface-Enhanced Raman Scattering," *Chemical Society Reviews* 27 (1998): 241.
53. D. A. K. Asamoto, G. Kang, and J. E. Kim, "Folding of the β -Barrel Membrane Protein OmpA into Nanodiscs," *Biophysical Journal* 118 (2020): 403–414.
54. S. A. Asher, "UV Resonance Raman Studies of Molecular Structure and Dynamics: Applications in Physical and Biophysical Chemistry," *Annual Review of Physical Chemistry* 39 (1988): 537–588.
55. S. Hashimoto, K. Obata, H. Takeuchi, R. Needleman, and J. K. Lanyi, "Ultraviolet Resonance Raman Spectra of Trp-182 and Trp-189 in Bacteriorhodopsin: Novel Information on the Structure of Trp-182 and Its Steric Interaction With Retinal," *Biochemistry* 36 (1997): 11583–11590.
56. T. Jordan, J. C. Eads, and T. G. Spiro, "Secondary and Tertiary Structure of the A-State of Cytochrome from Resonance Raman Spectroscopy," *Protein Science* 4 (1995): 716–728.
57. E. A. Milán-Garcés, S. Mondal, J. B. Udgaonkar, and M. Puranik, "Intricate Packing in the Hydrophobic Core of Barstar Through a CH– π Interaction," *Journal of Raman Spectroscopy* 45 (2014): 814–821.
58. R. P. Rava and T. G. Spiro, "Ultraviolet Resonance Raman Spectra of Insulin and α -Lactalbumin With 218 and 200-nm Laser Excitation," *Biochemistry* 1985 (1986): 24–1865.
59. K. M. Sanchez, T. J. Neary, and J. E. Kim, "Ultraviolet Resonance Raman Spectroscopy of Folded and Unfolded States of an Integral Membrane Protein," *Journal of Physical Chemistry B* 112 (2008): 9507–9511.
60. D. E. Schlamainger, M. M. Daschbach, G. W. Gokel, and J. E. Kim, "UV Resonance Raman Study of Cation– π Interactions in an Indole Crown Ether," *Journal of Raman Spectroscopy* 42 (2011): 633–638.
61. T. Takekiyo, L. Wu, Y. Yoshimura, A. Shimizu, and T. A. Keiderling, "Relationship Between Hydrophobic Interactions and Secondary Structure Stability for Trpzip β -Hairpin Peptides," *Biochemistry* 48 (2009): 1543–1552.
62. G. J. Thomas, "Raman Spectroscopy of Protein and Nucleic Acid Assemblies," *Annual Review of Biophysics and Biomolecular Structure* 28 (1999): 1–27.
63. Z. Q. Wen and G. J. Thomas, "Ultraviolet-Resonance Raman Spectroscopy of the Filamentous Virus Pf3: Interactions of Trp 38 Specific to the Assembled Virion Subunit," *Biochemistry* 39 (2000): 146–152.
64. X. Zhao, R. Chen, V. Raj, and T. G. Spiro, "Assignment of the 1511 cm^{-1} UV Resonance Raman Marker Band of Hemoglobin to Tryptophan," *Biopolymers* 62 (2001): 158–162.
65. H. Takeuchi, "Raman Structural Markers of Tryptophan and Histidine Side Chains in Proteins," *Biopolymers* 72 (2003): 305–317.
66. D. E. Schlamainger, J. E. Gable, and J. E. Kim, "Hydrogen Bonding and Solvent Polarity Markers in the UV Resonance Raman Spectrum

- of Tryptophan: Application to Membrane Proteins," *Journal of Physical Chemistry B* 113 (2009): 14769–14778.
67. I. Harada, T. Miura, and H. Takeuchi, "Origin of the Doublet at 1360 and 1340 cm^{-1} in the Raman Spectra of Tryptophan and Related Compounds," *Spectrochimica Acta A* 42 (1986): 307–312.
 68. T. Miura, H. Takeuchi, and I. Harada, "Tryptophan Raman Bands Sensitive to Hydrogen Bonding and Side-Chain Conformation," *Journal of Raman Spectroscopy* 20 (1989): 667–671.
 69. T. Miura, H. Takeuchi, and I. Harada, "Raman Spectroscopic Characterization of Tryptophan Side Chains in Lysozyme Bound to Inhibitors: Role of the Hydrophobic Box in the Enzymic Function," *Biochemistry* 30 (1991): 6074–6080.
 70. D. E. Schlaming, B. S. Leigh, and J. E. Kim, "UV Resonance Raman Study of TrpZip2 and Related Peptides: π - π Interactions of Tryptophan," *Journal of Raman Spectroscopy* 43 (2012): 1459–1464.
 71. P. C. Lee and D. Meisel, "Adsorption and Surface-Enhanced Raman of Dyes on Silver and Gold Sols," *Journal of Physical Chemistry* 86 (1982): 3391–3395.
 72. R. G. Parr and Y. Weitao, *Density-Functional Theory of Atoms and Molecules* (Oxford University Press Inc., 1995).
 73. Y. Zhao and D. G. Truhlar, "Density Functionals With Broad Applicability in Chemistry," *Accounts of Chemical Research* 41 (2008): 157–167.
 74. Y. Zhao and D. G. Truhlar, "The M06 suite of Density Functionals for Main Group Thermochemistry, Thermochemical Kinetics, Noncovalent Interactions, Excited States, and Transition Elements: Two New Functionals and Systematic Testing of Four M06-Class Functionals and 12 Other Functionals," *Theoretical Chemistry Accounts* 120 (2008): 215–241.
 75. M. Walker, A. J. A. Harvey, A. Sen, and C. E. H. Dessent, "Performance of M06, M06-2X, and M06-HF Density Functionals for Conformationally Flexible Anionic Clusters: M06 Functionals Perform Better than B3LYP for a Model System With Dispersion and Ionic Hydrogen-Bonding Interactions," *Journal of Physical Chemistry A* 117 (2013): 12590–12600.
 76. R. Ditchfield, W. J. Hehre, and J. A. Pople, "Self-Consistent Molecular-Orbital Methods. IX. An Extended Gaussian-Type Basis for Molecular-Orbital Studies of Organic Molecules," *Journal of Chemical Physics* 54 (1971): 724–728.
 77. C. Trujillo, A. Rodriguez-Sanz, and I. Rozas, "Aromatic Amino Acids-Guanidinium Complexes through Cation- π Interactions," *Molecules* 20 (2015): 9214–9228.
 78. M. Shakourian-Fard, H. Reza Ghenaatian, V. Alizadeh, G. Kamath, and B. Khalili, "Density Functional Theory Investigation Into the Interaction of Deep Eutectic Solvents With Amino Acids," *Journal of Molecular Liquids* 343 (2021): 117624.
 79. S. Miertuš, E. Scrocco, and J. Tomasi, "Electrostatic Interaction of a Solute With a Continuum. A Direct Utilization of Ab Initio Molecular Potentials for the Prediction of Solvent Effects," *Chemical Physics* 55 (1981): 117–129.
 80. M. J. Frisch, G. W. Trucks, and H. B. Schlegel, *Gaussian 09, Revision D.01* (Gaussian Inc., 2013).
 81. S. D. Dieng and J. P. M. Schelvis, "Analysis of Measured and Calculated Raman Spectra of Indole, 3-Methylindole, and Tryptophan on the Basis of Observed and Predicted Isotope Shifts," *Journal of Physical Chemistry A* 114 (2010): 10897–10905.
 82. H. Takeuchi and I. Harada, "Normal Coordinate Analysis of the Indole Ring," *Spectrochimica Acta A* 42 (1986): 1069–1078.
 83. B. Hernández, F. Pflüger, A. Adenier, S. G. Kruglik, and M. Ghomi, "Vibrational Analysis of Amino Acids and Short Peptides in Hydrated Media. VIII. Amino Acids With Aromatic Side Chains: L-Phenylalanine, L-Tyrosine, and L-Tryptophan," *Journal of Physical Chemistry B* 114 (2010): 15319–15330.
 84. C. Wu, M. Biancalana, S. Koide, and J. E. Shea, "Binding Modes of Thioflavin-T to the Single-Layer β -Sheet of the Peptide Self-Assembly Mimics," *Journal of Molecular Biology* 394 (2009): 627–633.
 85. M. Biancalana and S. Koide, "Molecular Mechanism of Thioflavin-T Binding to Amyloid Fibrils," *Biochimica et Biophysica Acta, Proteins and Proteomics* 2010 (2010): 1405–1412.
 86. M. Harel, L. K. Sonoda, I. Silman, J. L. Sussman, and T. L. Rosenberry, "Crystal Structure of Thioflavin T Bound to the Peripheral Site of *Torpedo californica* Acetylcholinesterase Reveals How Thioflavin T Acts as a Sensitive Fluorescent Reporter of Ligand Binding to the Acylation Site," *Journal of the American Chemical Society* 130 (2008): 7856–7861.
 87. G. Kumari, J. Kandula, and C. Narayana, "How Far Can We Probe by SERS?," *Journal of Physical Chemistry C* 119 (2015): 20057–20064.
 88. T. Maruyama and H. Takeuchi, "Effects of Hydrogen Bonding and Side-Chain Conformation on the Raman Bands of Tryptophan-2,4,5,6,7- d_5 ," *Journal of Raman Spectroscopy* 26 (1995): 319–324.
 89. S. P. A. Fodor, R. A. Copeland, C. A. Grygon, and T. G. Spiro, "Deep-Ultraviolet Raman Excitation Profiles and Vibronic Scattering Mechanisms of Phenylalanine, Tyrosine, and Tryptophan," *Journal of the American Chemical Society* 111 (1989): 5509–5518.
 90. J. A. Sweeney and S. A. Asher, "Tryptophan UV Resonance Raman Excitation Profiles," *Journal of Physical Chemistry* 94 (1990): 4784–4791.
 91. E. A. Milán-Garcés, S. Kaptan, and M. Puranik, "Mode-Specific Reorganization Energies and Ultrafast Solvation Dynamics of Tryptophan from Raman Line-Shape Analysis," *Biophysical Journal* 105 (2013): 211–221.
 92. E. C. Le Ru and P. G. Etchegoin, *Principles of Surface-Enhanced Raman Spectroscopy*, 1st ed., (Elsevier, 2009).
 93. E. C. Le Ru, S. A. Meyer, C. Artur, et al., "Experimental Demonstration of Surface Selection Rules for SERS on Flat Metallic Surfaces," *ChemComm* 47 (2011): 3903.
 94. J. S. Suh and M. Moskovits, "Surface-Enhanced Raman Spectroscopy of Amino Acids and Nucleotide Bases Adsorbed on Silver," *Journal of the American Chemical Society* 108 (1986): 4711–4718.
 95. A. G. Cochran, N. J. Skelton, and M. A. Starovasnik, "Tryptophan Zippers: Stable, Monomeric β -Hairpins," *Proceedings of the National Academy of Sciences of the United States of America* 98 (2001): 5578–5583.
 96. Y. Geng, T. Takatani, E. G. Hohenstein, and C. D. Sherrill, "Accurately Characterizing the π - π Interaction Energies of Indole-Benzene Complexes," *Journal of Physical Chemistry A* 114 (2010): 3576–3582.
 97. J. Grant Hill and A. Das, "Interaction in the Indole...Imidazole Heterodimer: Structure, Franck-Condon Analysis and Energy Decomposition," *Physical Chemistry Chemical Physics* 16 (2014): 11754.
 98. R. Van Lommel, T. Bettens, T. M. A. Barlow, J. Bertouille, S. Ballet, and F. De Proft, "A Quantum Chemical Deep-Dive into the π - π Interactions of 3-Methylindole and Its Halogenated Derivatives-Towards an Improved Ligand Design and Tryptophan Stacking," *Pharmaceuticals* 15 (2022): 935.
 99. Q. Tang, F. Zhu, Y. Li, et al., "Demonstration of π - π Stacking at Interfaces: Synthesis of an Indole-Modified Monodisperse Silica Microsphere $\text{SiO}_2@IN$," *Langmuir* 40 (2024): 8685–8693.
 100. S. M. Malathy Sony and M. N. Ponnuswamy, "Nature of π -Interactions in Nitrogen-Containing Heterocyclic Systems: A Structural Database Analysis," *Crystal Growth & Design* 6 (2006): 736–742.
 101. Y. Zhao, J. Li, H. Gu, et al., "Conformational Preferences of π - π Stacking Between Ligand and Protein, Analysis Derived from Crystal Structure Data Geometric Preference of π - π Interaction," *Interdisciplinary Sciences* 7 (2015): 211–220.

102. G. B. McGaughey, M. Gagné, and A. K. Rappé, “ π -Stacking Interactions,” *Journal of Biological Chemistry* 273 (1998): 15458–15463.
103. A. H. Hssain, T. Gomti Devi, R. O. Salih, and N. R. Abdullah, “Structural and Spectroscopic Study of L-Tryptophan Dimer State Using DFT and MD: Computational and Experimental Analysis,” *Journal of Molecular Structure* 1331 (2025): 141582.

Supporting Information

Additional supporting information can be found online in the Supporting Information section.